Chemical Engineering Journal xxx (xxxx) xxx–xxx

Contents lists available at ScienceDirect

Chemical Engineering Journal

journal homepage: www.elsevier.com/locate/cej

3D-CFD simulation of catalytic filter candles for particulate abatement and tar and methane steam reforming inside the freeboard of a gasifier

Elisa Savuto[a,*], Andrea Di Carlo[a], Katia Gallucci[a], Stefano Stendardo[b], Sergio Rapagnà[c]

[a] University of L'Aquila, Via Campo di Pile, L'Aquila, Italy
[b] ENEA, Casaccia Research Centre, 00100 Roma, Italy
[c] University of Teramo, Via R. Balzarini 1, 64100 Teramo, Italy

HIGHLIGHTS

- A 3D-CFD model of a fluidized bed gasifier with catalytic candles was developed.
- Simulations of tar steam reforming showed high temperature drop and low conversions.
- Small O_2 injections (~0.5 kg/h) were added in the freeboard to promote tar conversion.
- Simulations with low input tar, assuming fe-olivine bed, showed higher conversion.

ARTICLE INFO

Keywords:
3D-CFD modelling
Fluidized bed gasifier
Ceramic candle
Ni-catalyst
Catalytic gas conditioning
Tar abatement

ABSTRACT

Biomass gasification is a very promising process to produce energy from agricultural wastes; however, tar and particulate have to be removed in order to make the product gas exploitable. Catalytic filter candles inserted in the freeboard of a fluidized bed gasifier, perform hot syngas cleaning from particulate and promote the steam reforming reactions of tar and methane thanks to the addition of Ni-catalyst in their inner space. In this work, a 3D-CFD model is implemented in the FLUENT software, to simulate 6 catalytic candles housing in the freeboard of a pilot scale dual bubbling fluidized bed steam gasifier (100 kWth as biomass input). Main model parameters were derived from experimental results obtained with a bench scale gasification reactor, equipped with a ceramic filtering candle containing a commercial catalyst, to allow conditioning the raw syngas produced on site. Simulations were carried out to study the conversion of tar and methane in a real case application. The temperature drop along the gasifier freeboard causes very low conversion (≈15%) of tar produced inside the gasifier fluidized bed. It was found that small injections of O_2 in the freeboard can rise the temperature and increase tar conversion up to 77%. Finally, simulations with raw syngas input subjected to primary tar removal by means of Fe-olivine as fluidized bed material resulted in high conversion rates and residual tar content lower than 1 g/Nm^3.

1. Introduction

Biomass gasification is a very promising process to produce energy from agricultural wastes [1]; however, tar and particulate have to be removed in order to make the product gas exploitable. In order to meet the increasingly stringent environmental regulations, and increase the efficiency of biomass thermochemical conversion in useful gas and/or hydrogen syntheses, it is necessary to clean the product gas from particulate and tar [2].

The elimination of dust contained in the gas is compulsory before subjecting it to subsequent treatments such as reforming of high molecular weight hydrocarbons (tar) in light gases. Tar content in syngas produced in a fluidized bed gasifier ranges between 5 and 100 g/Nm^3 [3] and may cause different problems. For example, in the reformer units the catalysts might be deactivated as a consequence of carbon deposition; in the heat exchangers and turbines fouling and corrosion could represent a serious problem. Therefore, the gas cleaning units play an important role, also for the fly ash removal, in order to reach both environmental emission limits and protection of downstream units. Furthermore, the presence of tar among the products of gasification reduces gas yield and conversion efficiency. In addition, these contaminants are responsible for carbon deposition that can block

* Corresponding author.
E-mail address: elisa.savuto@univaq.it (E. Savuto).

https://doi.org/10.1016/j.cej.2018.10.227

1385-8947/

Nomenclature

Abbreviations

CFD	computational fluid dynamics
EDM	eddy dissipation model
SMR	steam methane reforming
WGS	water gas shift
m.u.	measurement unit

Symbols

A_j	pre-exponential factor of reaction *j* (R1…R8), m.u. see Table 3 and Table 5
c_i	molar concentration of specie i, kmol m^{-3}
C	inertial resistance factor, m^{-1}
C_{EDM}	empirical constant in eddy dissipation model
D	diameter of the insulation wall (in Eq. (20)), m
D_i	mass diffusivity of specie i, m^2 s^{-1}
D_{ik}	binary diffusion coefficient of species i, k, m^2 s^{-1}
E_j	activation energy of reaction *j* (R1…R8), J mol^{-1}
Gr	Grashof number
h	enthalpy, J kg^{-1}
h_{amb}	heat transfer coefficient, W m^{-2} K^{-1}
k	In Eq. (22) turbulence kinetic energy, m^2 s^{-2}
$k_{c,eff,g,ins}$	catalyst/candle, effective, gas, insulation thermal conductivity, W $m^{-1}K^{-1}$
k_j	rate constant of chemical reaction j (R1….R5), m.u. same of *A* see Table 5
K_j	arrhenius for adsorption group in reaction j (R3, R5), m^3 mol^{-1}
$K_{eq,j}$	equilibrium constant for reaction j (R1, R2), Pa^2 (R1) – dimensionless (R2)
M_i	molar weight of specie i, kg $kmol^{-1}$
Nu	Nusselt number
p	static pressure, Pa
p_i	partial pressure of specie *i*, Pa
Pr	Prandtl number
r_j	rate of reaction j (R1…R5), kmol kg^{-1} s^{-1}
$r_{j,EDM}$	eddy dissipation model rate of combustion reaction j (R6…R8), kmol m^{-3} s^{-1}
$r_{j,kin}$	kinetic rate of combustion reaction j (R6…R8), kmol m^{-3} s^{-1}
S_h	source term in the energy balance due to combustion reactions, J $m^{-3}s^{-1}$
S_i	source term in the balance of specie i due to combustion reactions, kg $m^{-3}s^{-1}$
T	temperature, K
v	velocity, m s^{-1}
x_k	molar fraction of specie k, mol mol^{-1}
y_i	mass fraction of species i, kg kg^{-1}

Greek letters

α	permeability, m^2
β_j	empirical constant for kinetic rate of combustion reactions
ΔH_{j0}	heat of reaction j, kJ $kmol^{-1}$
ε	In Eq. (22) rate of dissipation of turbulence energy, m^2 s^{-3}
ε_c	catalyst bed/candle porosity
η_i	empirical constant for kinetic rate of combustion reactions
μ	viscosity, kg m^{-1} s^{-1}
ν_{ij}	stoichiometric coefficient of species i in reaction j
ρ	gas density, kg·m^{-3}
ρ_{cat}	catalyst density, kg·m^{-3}
$\bar{\bar{\tau}}_g$	stress tensor, Pa m^{-1}

the porous media of a fuel cell anode. The tolerance limit of high temperature fuel cells to tars has yet to be fully defined in the literature due to the novelty of such systems and shortage of data on their long run performance; a value of the order of 100 ppm_w has however been proposed by Aravind and de Jong [4].

Catalytic filter candles are an innovative solution for hot gas cleaning and conditioning. The main advantage of this concept, differently from the low temperature gas purification systems, is that it avoids tar condensation and the operating temperature is closer to the gasification temperature [5]. Catalytic filter candles can be inserted directly in the freeboard of a fluidized bed biomass gasifier: in this way, particles removal, decomposition of tar and ammonia are integrated with gasification in one process unit [6], reducing thermal dispersion (especially for small scale applications) and increasing the overall efficiency of the process. Furthermore, the clean fuel gas is made available at temperature levels required by high efficiency power generation devices like high temperature fuel cells (SOFC or MCFC [7,8]) or to produce biofuels like bio-methanol [9] or synthetic natural gas [10,11] avoiding thermal losses.

Characterization of catalytic ceramic candles in terms of gas flow field, particle separation and tar reforming exhibited at different operating conditions has been the subject of a previous work [12] addressed to 2D-CFD simulations. Numerical results confirmed the experimental demonstration at lab and pilot scale that catalytic ceramic filters inserted in the freeboard of a fluidized bed gasifier, allow the complete removal of particulate by means of their anisotropic porous filtering structure, and furthermore act as an efficient media to remove tar (< 200 mg/Nm^3), thanks to the Ni catalyst impregnated into the filters body [13–19].

To by-pass technical problems related to the impregnation of Ni directly on the ceramic filters and to render the overall process more feasible in practice, commercial ceramic candles for particulate abatement at relatively high temperature could be filled with commercial pelletized steam reforming catalyst in their inner empty space. To verify this hypothesis, both, experimental and simulation work is required. In this paper, a 3D-CFD model was developed for the freeboard of a fluidized bed gasifier equipped with ceramic catalytic filters. To satisfy the filtration requirements of the raw gas produced by a pilot scale steam gasifier (100 kWth as biomass input) six full size, commercial filter elements are assumed to be arranged vertically above the fluidized bed, inside the reactor vessel, all of them filled with commercial pelletized steam methane reforming catalyst. Key model parameters (such as pre-exponential factors in the reforming reaction rate expressions, permeability and inertial resistance factor of filtering candle and inner catalyst bed) were first defined by means of experimental results obtained with the operation of a bench scale fluidized bed gasifier and then used to predict the behaviour of the tar conversion system in the pilot scale gasifier. The reactor was simulated assuming thermal dispersions towards the surrounding environment. In order to increase the gas temperature and consequently tar conversion in the candles, the injection of small amount of oxygen in the freeboard, burning a slight portion of the fuel gas, was also evaluated.

2. Experimental apparatus

The experimental data needed to validate the model and parameter values were obtained with a bench scale apparatus (see Fig. 1) composed of a bubbling fluidized bed gasifier with an internal diameter of 0.10 m and 0.87 m high, externally heated with a 6 kW electric furnace. The bed material consists of 3 kg of olivine with an average particle

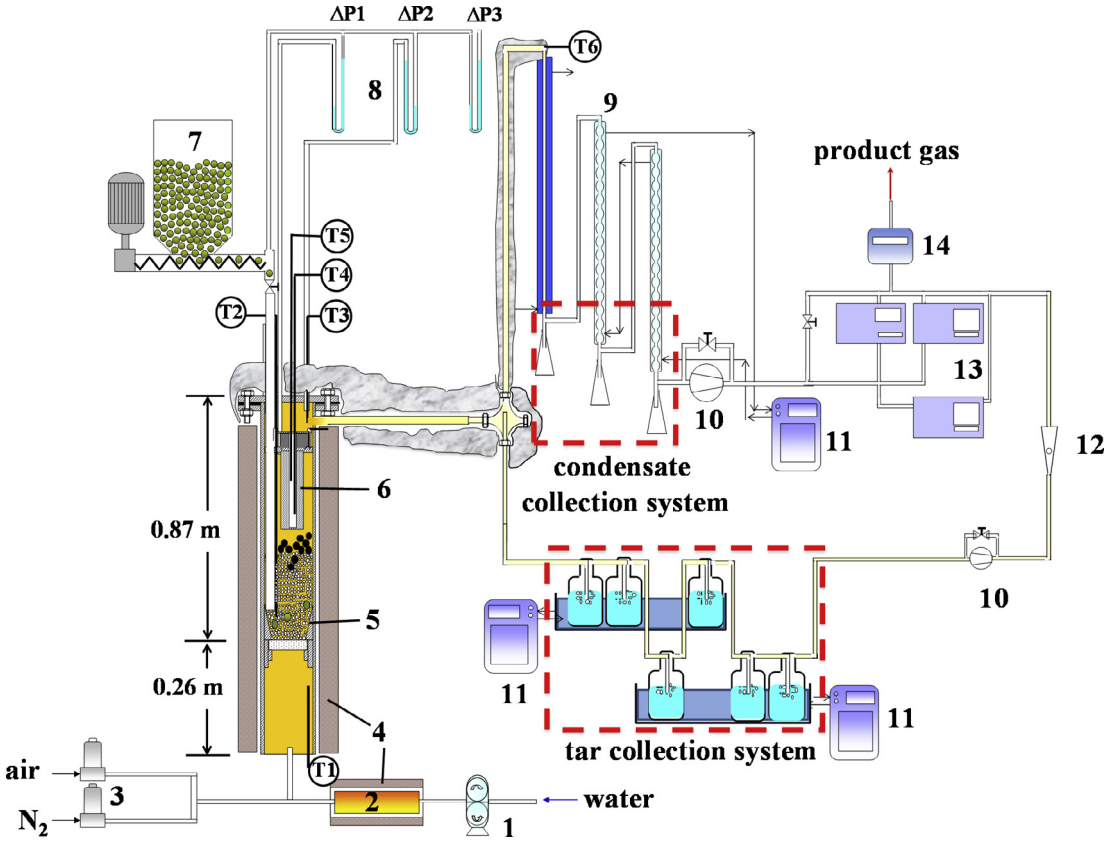

Fig. 1. Continuous fluidized bed biomass gasification bench plant. 1- water peristaltic pump; 2- steam boiler; 3-air and N_2 mass flow meters; 4- electric furnaces; 5-gasifier vessel ID 100 mm; 6- filter candle OD 60 mm, length of the filter candle segment 440 mm; 7-biomass feeder; 8-water manometers; 9-heat exchangers; 10-blowers; 11-chillers; 12-heater; 13-instant flow meter; 14-integral flow meter.

diameter of 360 μm and density 3000 kg/m^3. The upper part of the reactor was modified in order to insert a segment of a ceramic candle inside the freeboard; the ceramic filter, provided by PALL Schumacher GmbH, with an external diameter of 60 mm, an internal diameter of 40 mm, and a total filtration length of 440 mm (see Fig. 2a). The ceramic candle has an Al_2O_3 based asymmetric structure, with new improved candle support (UHT) characterized by coarse pores and a fine Al_2O_3 outer membrane layer on top of the support material, to separate fine particles (down to the order of one tenth of micron), with high efficiency.

The experimental tests were carried out feeding steam (Steam to Biomass ratio of 0.5 w/w) and nitrogen as fluidization medium in the wind-box. Steam was generated at 500 °C by feeding distilled water to a stainless steel evaporator electrically heated. Almond shell particles, 1.1 mm in Sauter mean diameter, were used as biomass feedstock. They were fed continuously into the hot fluidized bed at a constant rate in the range 4–11 g/min. All gasification tests were carried out at the same operating conditions and with the same biomass type and particle size. The gas stream at the gasifier outlet is cooled at room temperature by means of three condensers: the first one is made of stainless steel and is cooled with tap water; the others are made of glass with diethylene glycol solution as refrigerant; therefore the condensable fraction (water + tar) was separated from the gas and recovered in Erlenmeyer flasks.

Online gas analysers (IR, UV and TCD) were used for the real-time detection of H_2, CO, CO_2, CH_4, NH_3 and H_2S. In order to sample the tar produced by the gasification process, the technical specification CEN/TS 15,439 was applied on a slipstream of the product gas. The GC–MS analytical method was utilized to evaluate the tars present in each sample.

At the end of each gasification period, biomass feeding was stopped and air was injected into the gasifier to burn off the char. In this way, the quantity of char accumulated during the whole gasification period was determined by the analysis of CO_2 and CO in the exit gas. In order to check the catalytic activity of the filters located in the freeboard of the gasifier, two biomass gasification tests were performed and compared:

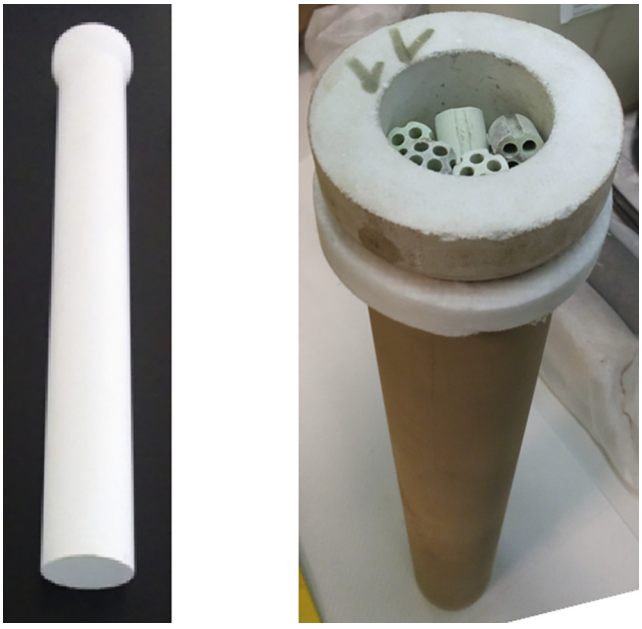

Fig. 2. a) ceramic candle; b) candle filled with commercial Ni-catalyst pellets.

Test I-blank test = olivine particles in the gasifier fluidized bed, and an Al_2O_3 based filter candle without catalyst in its freeboard;

Test II = olivine particles in the gasifier fluidized bed, and an Al_2O_3 based filter candle filled with catalyst in its freeboard (see Fig. 2b).

The main gasification conditions for the two tests are summarized in Table 1, while Table 2 shows the biomass composition.

Temperatures in various plant locations were measured by means of thermocouples, and measurement devices for the continuous monitoring of flow rates and pressure drop were also provided.

3. Development of the model

The system simulated by the model is the freeboard contained in a stainless steel (density: 8030 kg/m^3, specific heat: 502.48 J/(kg K), thermal conductivity: 25.1 W/(m K)) reactor vessel, above a dual bubbling fluidized bed (overall height 2.1 m), consisting of an internal cylindrical combustion reactor (0.22 m O.D.) fed with air, surrounded by a coaxial gasification reactor (0.44 m O.D.) fed with steam. In the gasification reactor six cylindrical catalytic candles (0.06 m O.D., 0.04 m I.D. 1.5 m length) are placed vertically and suspended from the top, for filtration and conditioning of the syngas generated there. More details about the characteristics of the catalytic ceramic candles can be found in [20]. The ceramic candles are defined as porous media made of alumina characterized by porosity and permeability. The internal volume in the candles was assumed to be filled with a packed bed made of commercial Ni-catalyst pellets for hydrocarbons steam reforming [21], additionally defined by its porosity and permeability. The gasification reactor is surrounded by a layer of 0.2 m of Insulfrax LT 128 ceramic blanket, an insulation material simulated as a solid region, as illustrated in Fig. 3.

The 3D-CFD numerical model was implemented in the FLUENT software. The chemical species considered are typical of a steam gasification gas product: H_2, CO, CO_2, CH_4, H_2O, and benzene (C_6H_6), toluene (C_7H_8) and naphthalene ($C_{10}H_8$). The tar key compounds taken into account in this work are well representative of the overall, complex tar mixture, since they are found in major quantity in a typical syngas produced from biomass gasification, as widely reported in the literature [22–26]. Even though the particulate matter contained in the product gas represents an issue and its removal is an important part of the gas cleaning and conditioning system, in this work its presence was neglected. A companion study of particulate filtration through ceramic candles was previously performed by Di Carlo and Foscolo [12], where an Eulerian–Lagrangian CFD model was developed and validated against experimental findings, to simulate the fluid dynamic behaviour of gas and solid particles inside the fluidized bed freeboard. The focus of this work is instead the catalytic conditioning of the gaseous phase by means of tar conversion.

The mass and momentum balances, given by the Navier-Stokes equations, chemical species and energy conservation equations are solved for the gas phase in the freeboard volume, in the porous zone of the candle and in the porous volume of catalyst pellets.

3.1. Freeboard region

For the freeboard region the following equations are solved for the gas phase:

$$\nabla\cdot(\rho\vec{v}) = 0 \tag{1}$$

$$\nabla\cdot(\rho\vec{v}\vec{v}) = -\nabla p + \nabla(\bar{\bar{\tau}}_g) \tag{2}$$

$$\nabla\cdot(\vec{v}(\rho h)) = \nabla\cdot[((\bar{\bar{\tau}}_g)\cdot\vec{v}) + k_g\nabla T] + S_h \tag{3}$$

$$\nabla\cdot(\vec{v}\rho y_i) = \nabla\cdot(D_i\nabla y_i) + S_i \tag{4}$$

where i indicates each of the chemical species. S and S_h are the source (or sink) terms due to any reaction occurring in the freeboard, if considered. These terms will be discussed later.

3.2. Porous structure of the filter candle and bed of catalyst pellets inside the candle

The continuity equation is similar to Eq. (1).

The momentum balance is similar to Eq. (2), modified to consider porosity (ε_c) of the solid (candle and catalyst bed) with an extra source term composed of two parts: a viscous loss term, that depends on permeability, α (Darcy law), and an inertial loss term (due to an inertial resistance factor C):

$$\nabla\cdot(\varepsilon_c\,\rho\vec{v}\vec{v}) = -\varepsilon_c\,\nabla p + \varepsilon_c\,\nabla\cdot(\bar{\bar{\tau}}_g) - \left(\frac{\mu}{\alpha} + \frac{C\rho}{2}\,|\vec{v}|\right)\vec{v} \tag{5}$$

Obviously, both α and C are different for the candle and for catalyst bed.

The conservation of energy for the gas, g, is expressed as follows:

$$\nabla\cdot(\varepsilon_c\vec{v}(\rho h)) = \nabla\cdot[k_{eff}\nabla T] + \sum_j r_j\rho_{cat}(1-\varepsilon_c)\Delta H_{j0} \tag{6}$$

where h is the sensible enthalpy for an ideal gas, involving only the sensible heat, ΔH_{j0} is the enthalpy of reaction j and k_{eff} is the effective thermal conductivity computed as:

$$k_{eff} = \varepsilon_c k_g + (1-\varepsilon_c)k_c \tag{7}$$

where k is the thermal conductivity of the gas phase, g, and of the catalyst/solid phase, c.

The following chemical species balance was finally set:

$$\nabla\bullet(\varepsilon_c\vec{v}\rho y_i) = \nabla\bullet(\varepsilon_c\rho D_i\nabla y_i) + \sum_j \nu_{ij} r_j\rho_{cat}(1-\varepsilon_c)M_i \tag{8}$$

In Eqs. (6) and (8) $\boldsymbol{r_j}$ is zero in the porous structure of the candle (where reactions can be considered negligible) and is different from zero only in catalyst bed.

The thermo-physical properties of the syngas were implemented in the model; its specific heat was calculated by the weighted average of the specific heat of its components.

The thermal conductivity and the viscosity of the syngas are polynomial functions of the temperature. A piecewise polynomial function was implemented to define the thermal conductivity and viscosity coefficients.

A k-ε model was adopted to model the gas turbulence in the freeboard of the simulated volume. The laminar flow model was used in the porous zones of the candle because the small pore diameters (in the order of 70 μm) guarantee very low Reynolds numbers (Re = 0.05–0.07).

The chemical-physical parameters integrated in the model for the porous layer of the candle and for the catalyst pellets were obtained from typical properties of alumina (density: 3939 kg/m^3, specific heat: 731.04 + 1.2119 T – 0.0007 T^2 J/(kg K), thermal conductivity: 34.274 – 0.0644 T + 4E-5 T^2 W/(m K)). The porosity of the candle structure (ε_{cand}) was set to 0.3, as reported by the manufacturer [20], while the porosity of the catalyst pellet (ε_{cat}) was set to 0.7, as that measured experimentally. The permeability and the inertial resistance factor of

Table 1
Gasification operating conditions.

Gasification Test	I (filtration candle without catalyst)	II (filtration candle with catalyst)
Duration of test (min)	100	140
Biomass flow rate (g/min)	11.25	11.41
Nitrogen flow rate (l/min)	18.27	17.8
Steam feeding rate (g/min)	5.81	6.29
Gasification Temperature (°C)	820	826

Table 2
Biomass (almond shells) proximate and ultimate analysis.

Proximate analysis % wt/wt (as received)		Elemental composition % wt/wt (dried at 105 °C)	
Dry matter	92.3	C	48.9
Ash	1.1	H	6.2
Volatile matter	71.7	N	0.18
Fixed carbon	19.5	O	43.5
		S	0.026

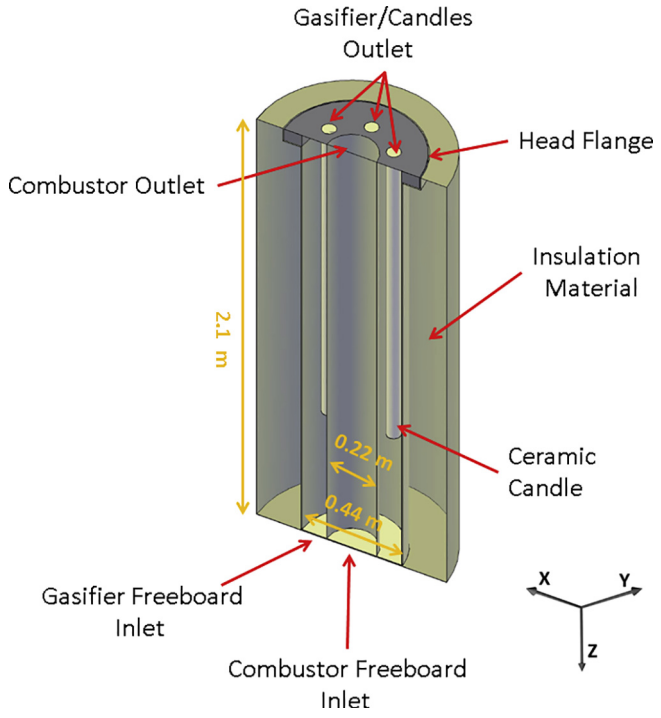

Fig. 3. CFD simulation control volume.

the candle porous body and of the inner catalytic bed were deduced by experimental measures of the pressure drop through the empty and catalyst-filled candle, for different temperatures and filtration velocities, in a previous work from the same authors [27].

The mass diffusivity of each component D_i was calculated with the Wilke equation [28]

$$D_i = \frac{1}{\sum_{k \neq i} \frac{x_k}{D_{ki}}} \tag{9}$$

where x_k are the molar fractions of different species.

The binary diffusion coefficient D_{ik} was calculated using the Chapman and Enskog [29] equation:

$$D_{ik} = 0.0018583 \sqrt{T^3 \left(\frac{1}{M_k} + \frac{1}{M_i}\right)} \frac{1}{p\sigma_{ik}^2 \Omega_{ik}} \tag{10}$$

where σ and Ω are the Lennard Jones parameters that can be found in Bird [29].

3.3. Reactions rates

The chemical reactions of tar and methane steam reforming and water gas shift taking place in the catalyst bed inside the candles were considered in the model;

$$CH_4 + H_2O \leftrightarrow 3H_2 + CO \tag{R1}$$

$$CO + H_2O \leftrightarrow H_2 + CO_2 \tag{R2}$$

$$C_6H_6 + 6H_2O \leftrightarrow 9H_2 + 6CO \tag{R3}$$

$$C_7H_8 + 7H_2O \leftrightarrow 11H_2 + 7CO \tag{R4}$$

$$C_{10}H_8 + 10H_2O \leftrightarrow 14H_2 + 10CO \tag{R5}$$

The reaction rate dependencies on concentrations (reaction order) and on temperature (activation energy) for the steam reforming of benzene and naphthalene were taken from Depner and Jess [30] that describes the catalytic conversion with a Nickel based catalyst (15% wt) in presence of H_2O, H_2 and traces of H_2S.

$$r_{R3} = \frac{k_{R3} c_{C6H6}}{1 + K_{R3} c_{C6H6} + K_{R3,H_2S} c_{H_2S}} \tag{11}$$

$$r_{R5} = \frac{k_{R5} c_{C10H8}}{1 + K_{R5} c_{C10H8} + K_{R5,H_2S} c_{H_2S}} \tag{12}$$

Swierczynski et al. [31] gave apparent first order kinetic parameters for the steam reforming of toluene over a Ni/olivine catalyst:

$$r_{R4} = k_{R4} c_{tol} \tag{13}$$

For the steam reforming of methane (SMR-R1) and the water gas shift reaction (WGS-R2), the model of Numaguchi and Kikuchi [32] with the kinetic parameters of de Smet [33] and the equilibrium constants of Hou and Huges [34] was used as the reference kinetic model:

$$r_{R1} = k_{R1} \frac{(p_{CH_4} p_{H2O} - p_{CO} {p_{H_2}}^3 / K_{eq,R1})}{{p_{H_2O}}^{1.596}} \tag{14}$$

$$r_{R2} = k_{R2} \frac{\left(p_{CO} p_{H2O} - \frac{p_{CO_2} p_{H_2}}{K_{eq,R2}}\right)}{p_{H2O}} \tag{15}$$

For Eqs. (11)–(15) the kinetic parameter k is expressed as a function of temperature by means of the Arrhenius dependency:

$$k_{Ri} = A_{Ri} e^{-ERi/RT} \quad i = 1, 2, 3, 4, 5 \tag{16}$$

3.4. Insulation region

The insulation region was simulated as a solid body. The only equation solved for this zone is the energy equation:

$$\nabla \bullet (k_{ins} \nabla T) = 0 \tag{17}$$

where k_{ins} is the thermal conductivity of the Insulfrax LT ceramic blanket [35] used for insulation (average values between Insulfrax LT 96 and 128, respectively), as a function of temperature:

$$k_{ins} = 2.05 \cdot 10^{-7} T^2 + 9.11 \cdot 10^{-5} T + 5.26 \cdot 10^{-2} \quad \frac{W}{mK} \tag{18}$$

At the outer wall of the solid region a heat flux boundary condition with ambient air was assumed:

$$k_{ins} \left(\frac{\partial T}{\partial n}\right)_{wall} = h_{amb} (T_{amb} - T_{wall}) \tag{19}$$

h_{amb} has been set to 5.7 W/m^{2}K according to the following correlation recommended by McAdams [36] for natural convection over a vertical cylinder for Grashoff number Gr $> 10^9$, as in the case of this work:

$$Nu = \frac{h_{amb} D}{k_g} = 0.13 (Gr \bullet Pr)^{1/3} \tag{20}$$

3.5. Combustion model

A positive action to improve tar conversion inside the candles is to increase the temperature in the freeboard and thus in the candles: in this way, the steam reforming reaction kinetics is accelerated. The combustion of a slight fraction of the fuel gas was therefore simulated,

injecting a small amount of oxygen at the gasifier outer surface, at different heights. In particular, 6 circumferential injection points were chosen at each height: 0.4 m (just below the candles), 0.8 m, 1.2 m and 1.6 m from the bottom of the reactor.

The reactions considered in this study are:

$$CH_4 + 1.5O_2 \rightarrow 2H_2O + CO \quad \text{(R6)}$$

$$CO + 0.5O_2 \rightarrow CO_2 \quad \text{(R7)}$$

$$H_2 + 0.5O_2 \rightarrow H_2O \quad \text{(R8)}$$

Because of the low concentration of the heavier hydrocarbons, the combustion of these species was neglected. Even if temperature can reach peaks higher than 1000 °C due to combustion and thus tar thermal cracking could be favoured at these temperatures, these reactions were also neglected in this work. This hypothesis (more conservative) is justified by the fact that temperature peaks are just hot spots in the entire fluid and the conversion of tar in these zones is surely negligible.

To simulate the combustion of syngas in the freeboard region, a finite rate/eddy dissipation model was used. Most fuels are fast burning, and the overall rate of reaction is controlled not only by Arrhenius-type kinetics (finite rate) but also by turbulent mixing. In non-premixed flames (like those evaluated in this work), turbulence slowly conveys/mixes fuel and oxidizer into the reaction zones where they burn quickly. The contribution of turbulent mixing can be evaluated adopting the eddy dissipation model proposed by Magnussen and Hjertager [37].

In the finite rate/eddy dissipation model adopted in this work both the Arrhenius-type finite rate ($r_{j,KIN}$), and eddy-dissipation reaction rate ($r_{j,EDM}$) are calculated. The net reaction rate r_j is taken as the minimum of $r_{j,KIN}$. and $r_{j,EDM}$.

The Arrhenius-type finite rate of the combustion reactions has the following expression:

$$r_{j,KIN} = T^{\beta j} A_j e^{-Ej/RT} \prod_i c_i^{\eta i} \mathrm{i} = H_2,\ CO,\ CO_2,\ H_2O,\ O_2 j = reactions\ R6 - R8 \quad (21)$$

β_j and ηi are empirical constants, A_j and E_j are pre-exponential factor and activation energy of the reaction j, respectively, c_k is the concentration of the specie k. The kinetic model developed by Westbrook and Dryer [38] was adopted for CH_4 and CO combustion, while that of Marinov et al. [39] for H_2 combustion. As confirmed by Wang et al. [40], the results obtained using these kinetic models are in good agreement with those obtained with a detailed reaction mechanism under hot and dilute oxidation conditions.

Table 3 shows parameter values used in the numerical simulations:

Being the flow rate of O_2 injected extremely low, according to the eddy dissipation model (EDM) of Magnussen and Hjertager, the rate of reaction j, is given by:

$$r_{j,EDM} = C_{EDM}\rho\frac{\varepsilon}{k}\left(\frac{y_{O2}}{\nu_{O2j}M_{w,O2}}\right) \quad (22)$$

where C_{EDM} is an empirical constant equal to 4.0.

As already mentioned, the minimum between $r_{j,KIN}$ and $r_{j,EDM}$ is chosen as net reaction rate r_j. The source (sink) terms S_i in the species balance (see Eq. (4)) are therefore calculated as:

$$S_i = M_i \sum_j \nu_{ij} r_j \quad (23)$$

where ν_{ij} are the stoichiometric coefficients of the specie i in the reaction j (negative for reagents and positive for products), M_i is the molecular weight of specie i, Furthermore, S_h in Eq. (3) is calculated as:

$$S_h = \sum_j r_j \Delta H_J \quad (24)$$

Since the temperature reached during the combustion, even if just in restricted hot spots, could be higher than 1000 °C, radiation must be also considered. For this reason a Discrete Transfer Radiation Model (DRTM) has been chosen, see Carvalho et al. [41] for more details. As reported by Ilbas [42], for the non-premixed combustion of a composite fuel (CH_4 and H_2), this model gives satisfactory results if compared with experimental values, for a geometry similar to those evaluated here and with the same turbulence model (k-ε) adopted in this work. As suggested by Ilbas, absorption coefficients used in the radiation model are 0.50 m^{-1} for the composite fuel, while scattering coefficients used are taken as 0.01 m^{-1}.

4. Model validation

In order to obtain reliable values for key parameters appearing in the model equations and validate the output of numerical simulations, experimental tests performed in the bench scale gasifier equipped with a single catalytic candle in its freeboard (Test I and Test II) were exploited. An axisymmetric integration domain was used in this case to simulate half of the cylindrical reactor represented in Fig. 1.

The inputs to the simulation were gas and tar compositions obtained in a biomass steam gasification test with a non-catalytic candle. The operating conditions were those used for the gasification tests: the gas input temperature was set to 820 °C, equal to the temperature measured in the reactor bed, and the upward superficial gas velocity was set to 0.365 m/s, that corresponds to a face filtration velocity of 100 m/h through the candle. A heat flux of 1300 W/m^2 was set on the reactor wall in order to reproduce the effect of the electric furnace used to heat the bench scale gasifier. The value chosen for the wall heat flux was assumed from enthalpy balances referred to the experimental tests. The temperature of the head wall of the reactor was set to 780 °C, equal to the value measured at the reactor outlet, near the candle head; the temperature measured there is most likely affected by thermal dispersions, corresponding to the top of the electric furnace (see Fig. 1). Two additional thermocouples, placed along the candle and immersed in the inner catalytic bed at 1/3 and 2/3 of its total length, allowed checking the reliability of the axial temperature profile calculated by the model (T4 and T5 in Fig. 1). Input composition and operating conditions are reported in Table 4.

Kinetic data for benzene, toluene, naphthalene, methane steam reforming and water gas shift found in literature [30–32] provided the functional dependencies of the respective reaction rates as functions of the concentration of species and temperature (activation energies). The simulation outputs, in terms of temperature profiles, gas composition, tar content and pressure drop, were compared with the results obtained in the experimental tests carried out in the bench scale reactor equipped with a ceramic candle filled with commercial Ni-catalyst pellets for steam reforming of hydrocarbons. In particular, the comparison between predicted and experimental values of tar content in the output gas stream allowed estimating the pre-exponential factors of the kinetic constant in each reaction rate expression needed to obtain simulation results close to the experimental outcomes. The chosen pre-exponential factors are reported in Table 5.

The simulation results finally obtained are shown in Fig. 4 and Table 6.

As shown in Fig. 4, model calculations allowed predicting

Table 3
Different global combustion mechanisms with kinetic rate data.*

	A	β	E/R (K)	Reaction orders
R6 [38]	$5.03{\cdot}10^{11}$	0	24,056	$[CH_4]^{0.7}[O_2]^{0.8}$
R7 [38]	$2.24{\cdot}10^{12}$	0	20,484	$[CO][O_2]^{0.25}[H_2O]^{0.5}$
R8 [39]	$5.69{\cdot}10^{11}$	0	17,609	$[H_2][O_2]^{0.5}$

* Units in kmol, m^3, K, s.

Table 4
Gasifier freeboard input compositions (Test I) and operating conditions for simulation.

Input composition	
H2 (%vol dry, N2 free)	40.04
CO (%vol dry, N_2 free)	29.05
CO_2 (%vol dry, N_2 free)	22.35
CH_4 (%vol dry, N_2 free)	8.56
H_2O content (%)	15.67
C_6H_6 (g/Nm^3)	10.40
C_7H_8 (g/Nm^3)	2.30
$C_{10}H_8$ (g/Nm^3)	2.04
H_2S (ppm_v)	100
Operating conditions	
T in (°C)	820
Wall heat flux (W/m^2)	1300
v in (m/s)	0.365

Table 5
Values of pre-exponential factors adopted in the chemical reaction rate expressions.

Reactions	Pre-exponential factors
$CH_4 + H_2O \leftrightarrow CO + 3H_2$	36.79 kmol/m^3 Pa$^{-0,404}$/s
$CO + H_2O \leftrightarrow CO_2 + H_2$	3.51E-5 kmol/m^3 Pa$^{-0,404}$/s
$C_6H_6 + 6H_2O \leftrightarrow 6CO + 9H_2$	6309 s^{-1}
$C_7H_8 + 7H_2O \leftrightarrow 7CO + 11H_2$	4.44E10 s^{-1}
$C_{10}H_8 + 10H_2O \leftrightarrow 10CO + 14H_2$	8.67E8 s^{-1}

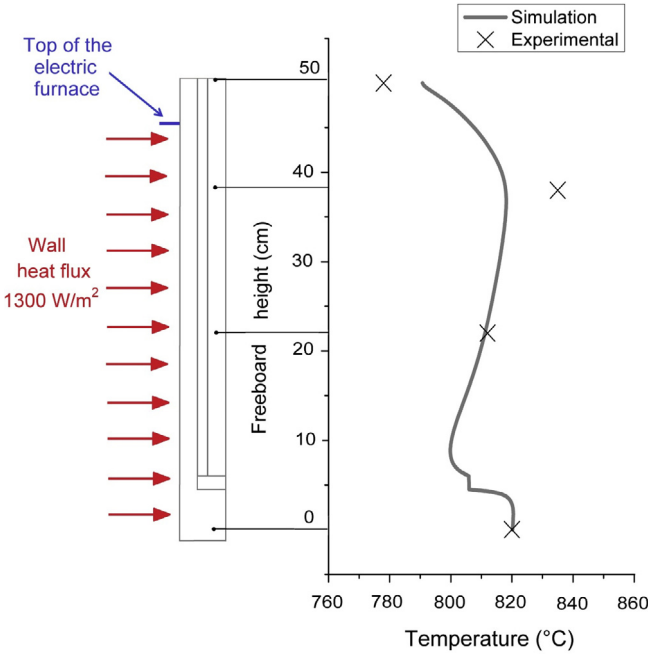

Fig. 4. Comparison of experimentally measured temperature values and axial temperature profile predicted by the simulation model, inside the reactor freeboard below the filtration candle and then in the candle inner catalytic bed.

temperature as a function of reactor height, inside the fluidized bed freeboard, across the bottom wall of the filter candle and along its inner catalytic bed up to the output gas stream; this profile is compared with the experimental values measured at the corresponding heights.

As reported in Fig. 4, a temperature of approximately 810 °C was measured in the lower point of the catalytic bed; this temperature decrease compared to the input value is most likely ascribable to the endothermic steam reforming reactions that take place mainly in the lower part of the candle because of the high temperatures and concentrations of tar and methane. In the upper part of the catalytic bed, the measured temperature is higher, about 835 °C, probably because of the minor extent of the steam reforming reactions there, which thus require less heat flux. At the outlet of the reactor the temperature strongly decreases, because of the thermal dispersions close to the head of the gasifier, reaching a value of approximately 780 °C.

The Figure also shows that the model reproduces well this trend: the calculated temperature values are fairly close to the experimental values measured at different points, so that inputs and conditions used for simulation can be considered representative of the phenomena occurring in the real bench scale gasifier during a catalytic test.

Table 6
Comparison of experimental and simulation results.

	Experimental output	Simulation output
H_2 (%vol dry, N_2 free)	53.75	48.42
CO (%vol dry, N_2 free)	23.89	29.11
CO_2 (%vol dry, N_2 free)	18.63	19.34
CH_4 (%vol dry, N_2 free)	3.73	3.13
C_6H_6 (g/Nm^3)	4.93	3.31
C_7H_8 (g/Nm^3)	0.95	0.69
$C_{10}H_8$ (g/Nm^3)	0.85	0.56
T out (°C)	778	790
Pressure drop at v_{filtr} = 100 m/h (mbar)	39.2	45

Table 6 shows that the experimental values of tar content resulting from the catalytic treatment are well reproduced by the simulation model. A satisfactory correspondence is also obtained between simulated and experimental concentration values of gaseous species: major discrepancies concern H_2 (-9% relative error) and CO (+23%), respectively. It should be considered here that in each catalytic test performed with the bench scale rig, the gas composition in the reactor freeboard surrounding the candles (i.e. the inlet boundary condition for the computation model) cannot be measured and therefore known precisely; in simulations, it was inferred from the results of a blank gasification test without catalyst pellets in the ceramic candle. Oscillations in the abundance of the atomic species are always possible among different gasification runs at close operating conditions: this can well explain discrepancies as those reported in Table 6. Anyway this difference in CO values does not affect the validity of the model regarding tar conversion.

5. Results and discussion

The 3D-CFD model was then used to simulate tar conversion in the freeboard of the dual bubbling fluidized bed steam gasifier integrated with six catalytic candles. The input gas composition used for these simulations were taken from the results recorded in the 100 kWth pilot scale dual fluidized bed gasifier operated at Vienna University of Technology, here assumed as reference values of gas composition in a dual fluidized bed steam gasifier [43]. N_2 (10% in volume) was added to the input gas composition, assuming a small leakage between the combustion and gasification chambers of the reactor. Input tar compositions were taken from a previous work [18]. The input gas and tar composition are summarized in Table 7.

For the insulation wall, an ambient temperature of 300 K and a heat transfer coefficient of 5.7 W/m^2 K were set (see Eqs. (19) and (20)).

Results of simulations with the above mentioned input parameters are reported in Fig. 5.

Fig. 5 also shows the gas temperature calculated at the outlet of the ceramic candles: the value estimated by the model is close to that at the top of the candles outer surface. The estimated tar conversion yields obtained in this simulation are in the range of 10–20%, and thus the tar residual content is still too high for an effective exploitation of the syngas (~10 g/Nm^3, excluding benzene). Furthermore, it was observed

Table 7
Input composition and operating conditions used in simulations.

	Gasifier input	Combustor input
H_2 (%vol dry, N_2 free)	38.70	
CO (%vol dry, N_2 free)	20.29	
CO_2 (%vol dry, N_2 free)	30.57	CO_2 %vol 8.68
CH_4 (%vol dry, N_2 free)	10.43	N_2 %vol 70.12
H_2O content (%)	23.39	H_2O %vol 21.20
C_6H_6 (g/Nm^3)	11.00	–
C_7H_8 (g/Nm^3)	8.00	–
$C_{10}H_8$ (g/Nm^3)	4.60	–
Operating conditions		
T gas in the fluidized bed (°C)	850	950
Input gas flow (Nm^3/h)	18.19	26.55

that the temperature strongly drops along the reactor height, reaching 679 °C at the outlet of the candles, this being probably the cause of the low tar conversion rate; tar steam reforming over Ni catalysts is in fact effective at temperatures higher than 700 °C [44,45].

As also shown in Fig. 5, temperature on the gasifier wall is lower than that on the catalytic filter candles at the same freeboard height, so that it can be inferred from this simulation that heat dispersions are the major cause of the temperature drop, much more than the endothermic steam reforming reactions in the catalytic packed bed contained inside the candles, the extent of which is quite limited in this case. From rough calculations on the heat fluxes, it is indeed found that the thermal dispersion fluxes are 1.5–2 times higher than the thermal power demand linked to the progression of the endothermic steam reforming reactions, confirming the observations made above.

More insight on temperature distribution predicted by the model in the whole reactor freeboard, in the body of the filtering candles and in the inner catalytic fixed bed is provided by Fig. 6, together with radial temperature profiles in different sections of the candle; a comparison is also made with the temperature distribution map computed when all reforming reactions are suppressed, other operating conditions being equal.

Fig. 6 shows the profiles of temperature along an x-z oriented surface passing through the centre of two candles, and in three sections (A, B and C) at different heights of the candle. It is possible to observe that in presence of the endothermic steam reforming reactions, the temperature profiles along the surface are different compared to the case where these are absent; in particular, a decrease of the temperature values towards the upper part of the candle is noticed. This effect is confirmed by the radial temperature profiles at different heights of the candle; between sections A and C there is indeed a temperature difference of approximately 80 K. It was also observed that in section C, in which the temperature is higher, temperature tends to decrease towards the centre of the candle, probably due to the demand of heat by the steam reforming reactions that take place in the catalytic volume. Section A instead, in the upper part of the candle, shows a different trend with temperature decreasing towards the external part of the reactor (upper-right side of the section); this effect could suggest that thermal dispersions would prevail there on heat absorption by a low extent of the steam reforming reactions.

Fig. 7 shows the reaction rates of methane and naphthalene steam reforming; the values refer to three radial sections, A, B and C, at different heights of the candle.

Differences among the values of reaction rates, in the external as well as in the internal part of the catalytic bed were noticed, especially in section C. In particular, the peripheral part of each section shows comparatively higher values, both for naphthalene and for methane steam reforming reaction rates. In addition to the effect of the radial temperature distribution that is particularly important in section C (Fig. 6), this outcome of the model derives from the combination of flow, composition and temperature fields at different heights of the catalytic bed.

Furthermore, methane and naphthalene show the highest values of reaction rates in the lower section of the candle (C), while in the upper sections the values are strongly reduced; section A shows indeed reaction rates reduced of nearly one order of magnitude for naphthalene and of 2.5 times for methane, compared to section C. This phenomenon is certainly ascribable to the temperature variations along the candle, specifically the substantial temperature drop predicted towards the exit of the reactor. It is thus found that the control of temperature and the reduction of thermal losses are crucial issues in the chemical reaction design for tar removal.

The solution suggested to answer properly the above issues consists in blowing a small flowrate of O_2 in the freeboard of the reactor, in order to burn a little portion of the fuel gas, and increase the temperature enough to promote the tar reforming reactions. A distributed oxygen feeding system was implemented in the model of the gasifier freeboard, made of four series of nozzles uniformly positioned around the reactor circular wall, each made of six nozzles, located at different

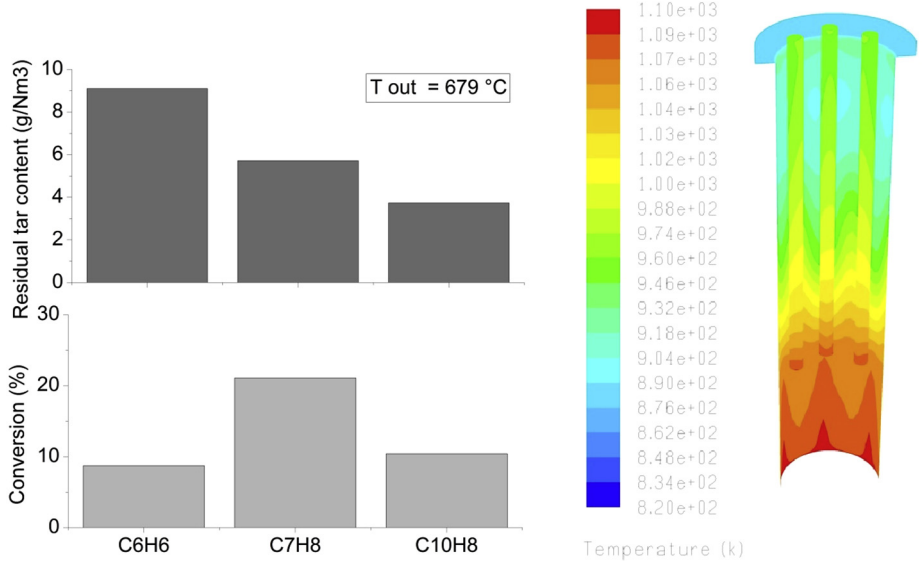

Fig. 5. a) Tar conversion and residual tar content in the product syngas; b) Temperature profiles at the inner wall of the reactor steel vessel, at the outer surface of ceramic candles and on the steel top flange.

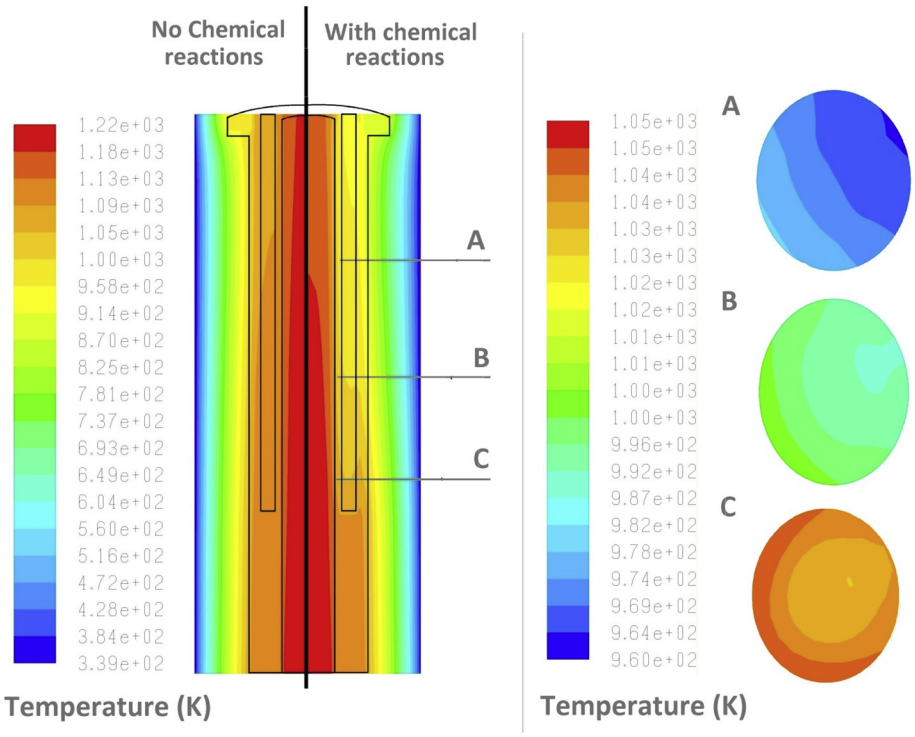

Fig. 6. Comparison of axial temperature profiles without and with chemical reactions (left); radial temperature profiles at different heights inside the catalytic candle, with chemical reactions (right).

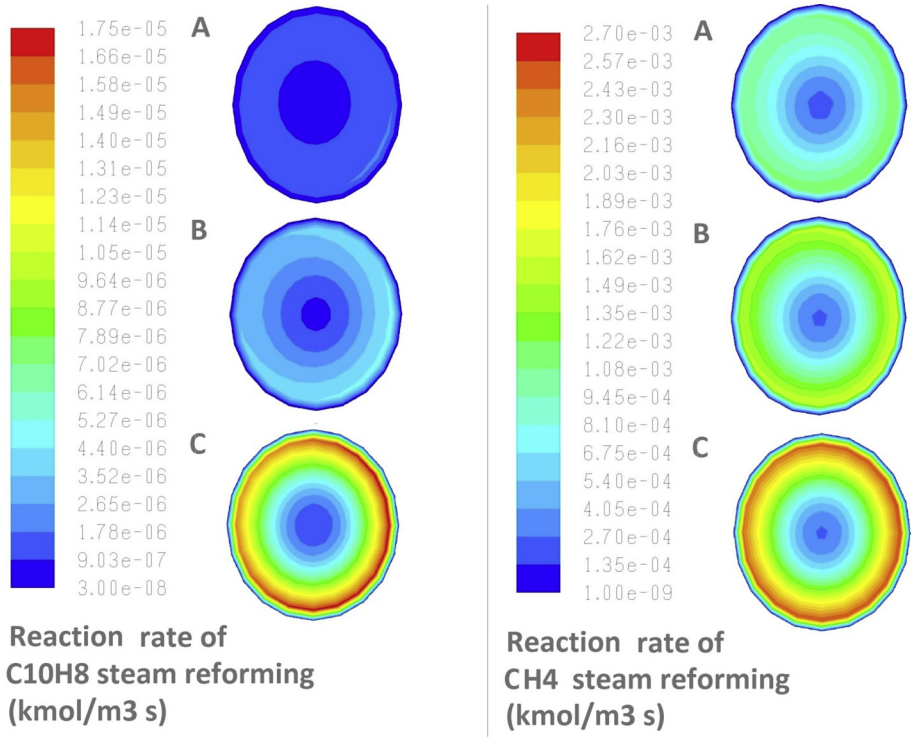

Fig. 7. Reaction rates of naphthalene (left) and methane (right) steam reforming on horizontal cross sections A, B and C of the catalytic bed inside the filter candle.

heights in the simulated volume (0.4 m, 0.8 m, 1.2 m and 1.6 m from the bottom of the reactor). Fig. 8 shows the volume simulated with the cylindrical nozzles for oxygen injection (the cylinder of the combustor is not shown for clarity).

Simulations were carried out with different O_2 flows (0.12, 0.36 and 0.60 kg/h corresponding respectively to 1, 3 and 5 wt% of the O_2 contained in the air input flow rate fed to the combustion reactor), in order to investigate the best solution in terms of tar conversion and gas composition. The results are displayed in Fig. 9 and 10.

The numerical results show that the outlet temperature and the tar conversion are enhanced thanks to the O_2 injections; in particular it is observed that injection of 1% of the O_2 sent to the combustor leads to conversion rates ranging between 50 and 60%, while injections corresponding to 3% show tar conversion rates around 75–80%. Injections of

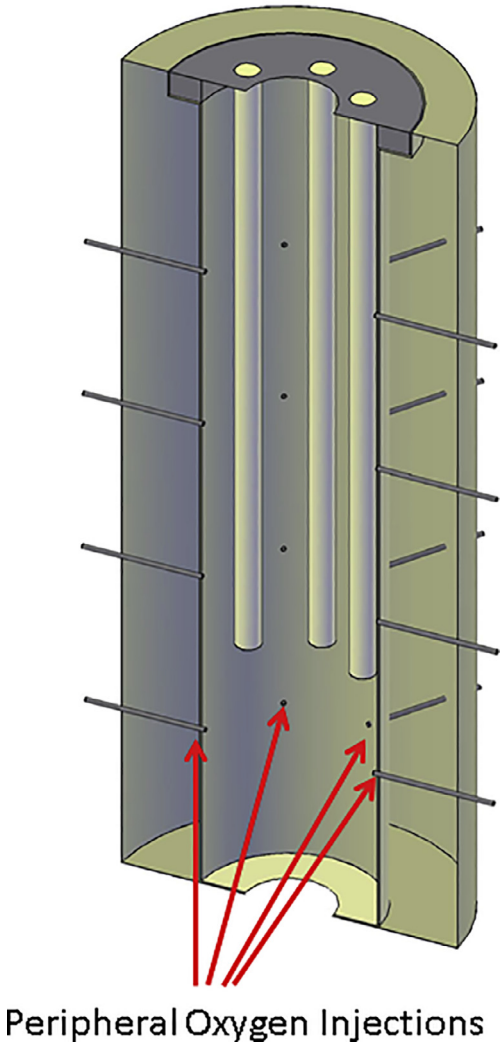

Fig. 8. Simulated volume with nozzles for O_2 injections.

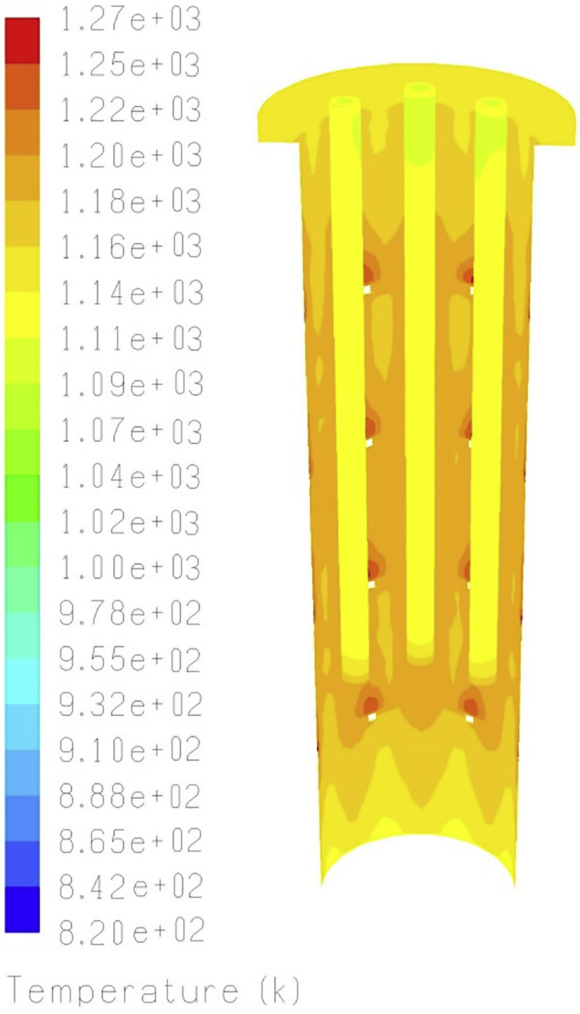

Fig. 10. Temperature profiles with O_2 injections (3% of the O_2 flow to the combustor).

O_2 equal to 5% of the O_2 sent to the combustor show slightly higher conversion rates compared to the results obtained with 3%, ranging between 78 and 85%. The diagram showing the residual tar content confirms that the cases at 3 and 5% lead to around 2 g/Nm^3 of tar in the nitrogen free, dry product gas, while the case at 1% leads to above 4 g/Nm^3. Moreover, Fig. 10 shows that with O_2 injections in the freeboard, the temperature profiles along the candles is much more uniform, and the temperature difference between the lower and the upper part of the filters is almost eliminated.

Fig. 11 reports the temperatures along an x-z oriented surface passing through the centre of two candles, and the temperature profiles in three sections of the candle at different heights, in presence of small oxygen injections. The profiles show that in this case the temperature along the reactor and thus the candle is definitely more uniform, thanks to the injections of oxygen that compensate the effect of the thermal losses in the upper part of the reactor. This observation is also confirmed by the temperature profiles on the horizontal cross sections, which show a temperature difference between sections A and C of only

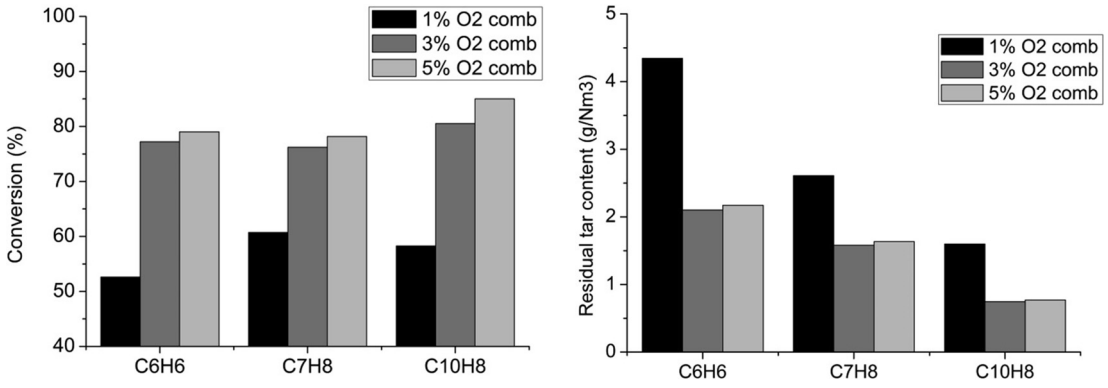

Fig. 9. Results of simulation with different O_2 injections (1, 3 and 5% of the O_2 flow to the combustor).

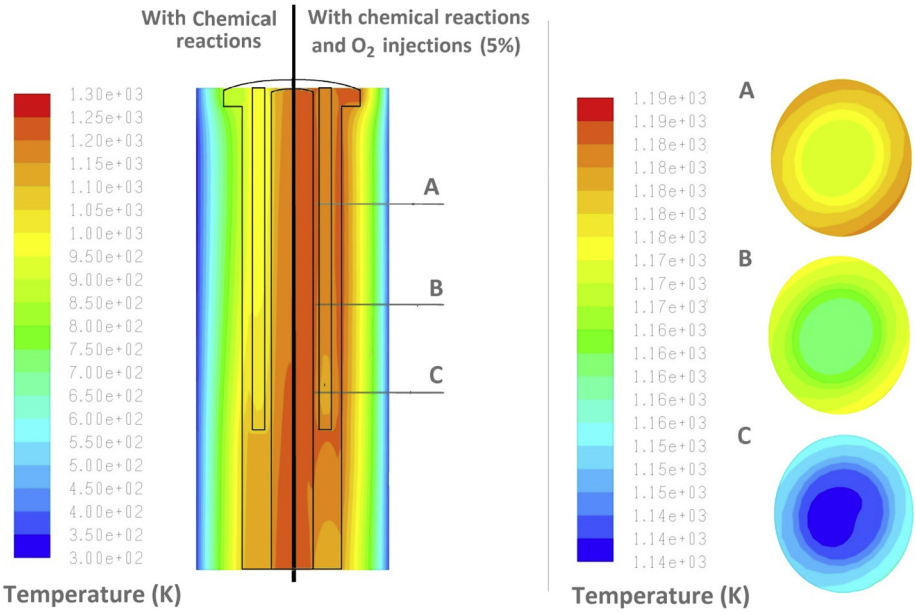

Fig. 11. Comparison of axial temperature profiles with chemical reactions and with O_2 injections in addition (left); radial temperature profiles at different heights inside the catalytic candle, with O_2 injections (right).

20 K on the external part of the candle, much lower than that reported in Fig. 6 (80 K). Furthermore, all three sections show temperature profiles decreasing towards the centre of the candle, indicating a likely, significant extent of endothermic steam reforming reactions over the whole candle length.

Fig. 12 shows the reaction rates of methane and naphthalene on horizontal cross sections at different heights of the candle; it can be observed that the reaction rates of methane and naphthalene steam reforming exhibit a more uniform path among the lower and upper sections of the candle, contrarily to what shown by the previous results obtained in the absence of oxygen injections.

As already noticed in Fig. 7, the reaction rates have relevant values mostly in the external layers of the catalytic candle, and the concentration of methane and naphthalene rapidly drop towards the interior of the candle, as shown in all sections reported here. As a result, in the internal part of the candle the reaction rates are very low, about 1E-8 kmol/(m^3 s) for naphthalene and 2E-4 kmol/(m^3 s) for methane.

The partial combustion of the gas compounds with the injected O_2 causes a higher content of CO_2 in the final gas composition, which leads to a reduction of the energy content of the gas. Table 8 shows the outlet

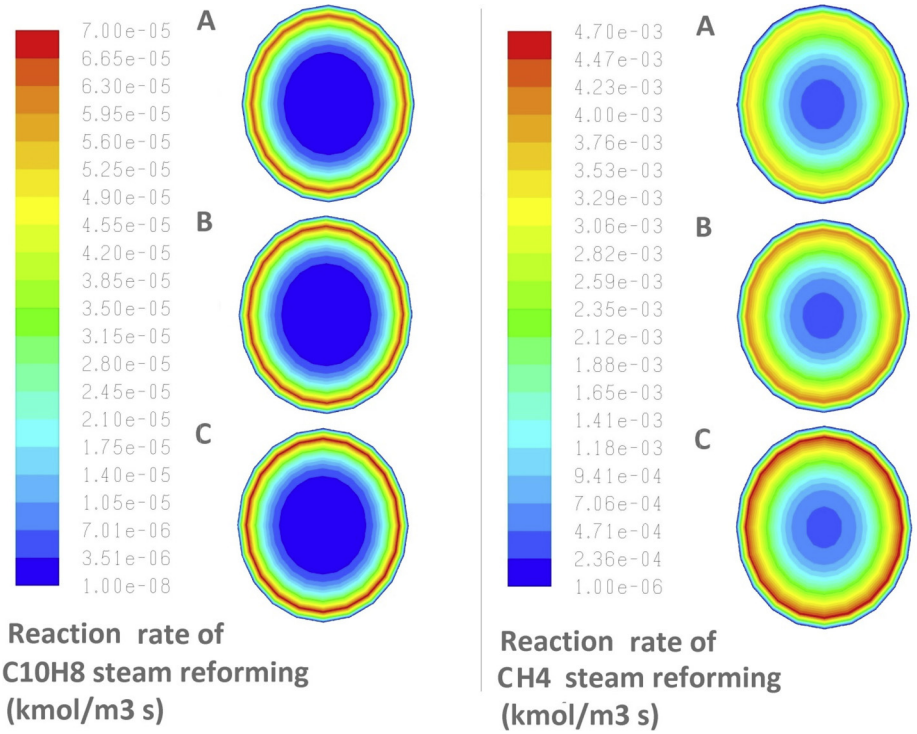

Fig. 12. Reaction rates of naphthalene (left) and methane (right) steam reforming on horizontal cross sections A, B and C of the catalytic bed inside the filter candle, in presence of small oxygen injections.

Table 8
Temperature and LHV of gas at the outlet of the ceramic candles.

O_2 additional input	0	1% of O_2 comb.	3% of O_2 comb.	5% of O_2 comb.
O_2 flow rate (kg/h)	–	0.12	0.36	0.60
T out (°C)	679	789	833	877
LHV (MJ/Nm^3)	7.21	7.05	6.83	6.60

temperatures and the lower heating values of the product gas, in cases with different injected flows of O_2. The case with oxygen injection corresponding to 3% of the O_2 fed to the combustor seems to be a good compromise for fairly high tar conversion values, with a corresponding small loss of energy content.

Even though the O_2 injections improved the tar conversion, the residual tar content is still too high for the final utilization of the product gas: the threshold values for tar should be close to 100 ppm_w. Therefore, it was concluded that the commercial catalyst for hydrocarbon steam reforming considered here cannot guarantee the needed tar conversion performance, with the input tar content assumed in this case; future studies should thus be focused on testing different commercial catalysts, particularly suitable for the steam reforming of heavy hydrocarbons.

An alternative process option for the hot gas catalytic conditioning, worth to be investigated here, consists in a more efficient combination of primary and secondary measures for tar abatement, focusing on the enhancement of tar conversion inside the gasifier fluidized bed, obtained by means of a bed material with catalytic activity higher than that of olivine [46]. In this way, reducing the input tar content in the gas flowing to the catalytic candles, the performance of the catalyst could be enhanced. Previous experimental work, carried out with the same bench scale rig described in this work, includes biomass gasification tests with Fe-olivine as bed material, i.e. enriching the content of free iron oxides of natural olivine by impregnation [47]; as a matter of facts, it is well known that iron oxides are an effective catalyst of gasification [48]. That experimental work confirmed tar reduction directly inside the gasifier bed, producing a gas with lower tar content. Those results were here used as inputs for additional simulations assuming Fe-olivine as bed material in the dual bubbling fluidized bed equipped with the catalytic candles. The input conditions for this simulation are summarized in Table 9.

It is worth noticing that, together with a lower tar content in the raw syngas input to the filtering candles, this time a steam concentration higher than that in the gasification tests described previously is also present (see Table 7), because of a greater value of the steam/biomass ratio (1.2 instead of 0.5) [47]. This circumstance should not prevent comparison with the performance of catalytic filtering candles predicted for previous tests, because the steam content of the input raw syngas is in remarkable excess in both cases, in relation to its consumption by chemical reactions taking place inside the candles; the influence of a larger H_2O excess in the kinetic rate expressions (see Eqs. (14) – (16)) is quite negligible [47]. This is also confirmed by the experimental results obtained by Garcia-Labiano et al. [19]. In their work a small segment of a catalytic ceramic candle (Ni based) was tested at a uniform temperature of 800 °C, with a gas obtained by steam gasification of biomass, using Fe/olivine as bed material and at different steam to biomass ratios (between 0.55 and 0.88). Their results showed that tar conversion is always between 60 and 80 %.

The numerical results obtained are summarized in Fig. 13.

The results show that, in comparison with the previous case (a gasifier bed made of plain olivine, Fig. 5), the temperature drop along the catalytic candles is lower, causing a gas outlet temperature of 748 °C, and higher tar conversions rates are obtained, between 35 and 50%. The residual tar content in fact is strongly reduced: the sum of toluene and naphthalene is about 1.8 g/Nm^3. It is thus deduced that with a lower initial tar content, the catalyst shows a better performance, closer to that expected for a complete gas conditioning process.

However, tar concentration threshold limits for the utilization of fuel gas in fuel cells are not yet obtained; therefore a simulation with Fe-olivine as bed material combined with small injections of O_2 was also carried out. The O_2 flow chosen was 0.065 kg/h, corresponding to 0.5% of the O_2 flow sent to the combustor, in order to affect as little as possible the energy content of the gas. The results of the simulation are shown in Fig. 14.

The simulation with Fe-olivine as bed material and small O_2 injections shows the best results obtained so far: tar conversion rates range between 64 and 68% and the residual tar content is around 0.9 g/Nm^3 (naphthalene + toluene), a value close to the threshold limit for feeding solid oxide fuel cells. Similarly to what observed in the previous case with O_2 injections, the profiles show that the temperature is much more uniform along the whole candles length.

Although the outlet temperature is around 790 °C, still the tars did not reach complete conversion. The contact time is probably too short for an effective steam reforming of heavy hydrocarbons, with the catalyst activity considered here. It should be also taken into account the very high porosity of catalyst pellets (70%, as mentioned above) that reduces the mass of catalyst charged in each candle. Even though the catalytic primary treatment with the bed material and O_2 injections have shown enhancement in tar reduction, the availability of catalysts more active for reforming of heavy molecular weight hydrocarbons remains an open issue.

6. Conclusions

A 3D-CFD model describing steam reforming of hydrocarbons in the freeboard of a dual bubbling fluidized bed gasifier equipped with catalytic candles was developed utilizing constitutive equations proposed by the authors.

To validate the model the simulation outputs were compared with all available data obtained from real gasification tests at lab scale, utilizing a segment of a commercial candle filled with a commercial catalyst. The model validation performed on the base of experimental values of syngas temperature axial profile, tar content and composition, gas composition and overall pressure drop through the conditioning system were considered sufficient to obtain reliable predictions of the operation of the pilot scale gasifier.

Simulations showed the importance for the reforming process of the temperature distribution in the reactor freeboard, in the candle body and in the inner catalyst bed as well as the sensitivity of the model to temperature variations. The results demonstrated that there is a consistent temperature drop along the height of the freeboard, which causes rather low temperature of the filter candles and the consequent low tar conversion (around 10–20%). Several simulations were carried out in order to identify a solution to the issue of temperature drop, mainly caused by heat dispersions at the gasifier wall; different flows of

Table 9
Input composition and operating conditions of simulation with Fe-olivine primary tar removal.

	Gasifier input	Combustor input
H_2 (%vol dry, N_2 free)	53.00	
CO (%vol dry, N_2 free)	27.00	
CO_2 (%vol dry, N_2 free)	14.00	CO_2 %vol 8.68
CH_4 (%vol dry, N_2 free)	6.00	N_2 %vol 70.12
H_2O content (%)	42.45	H_2O %vol 21.20
C_6H_6 (g/Nm^3)	3.14	–
C_7H_8 (g/Nm^3)	1.65	–
$C_{10}H_8$ (g/Nm^3)	1.45	–
Operating conditions		
T in (°C)	850	950
Input gas flow (Nm^3/h)	18.19	26.55

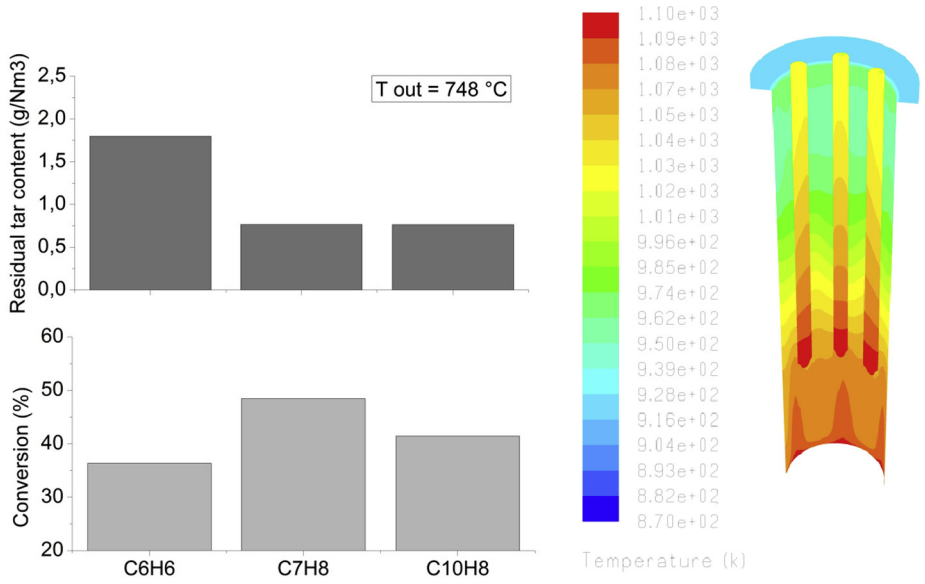

Fig. 13. a) Tar conversion and residual tar content in the product syngas; b) Temperature profiles with Fe-olivine in the fluidized bed.

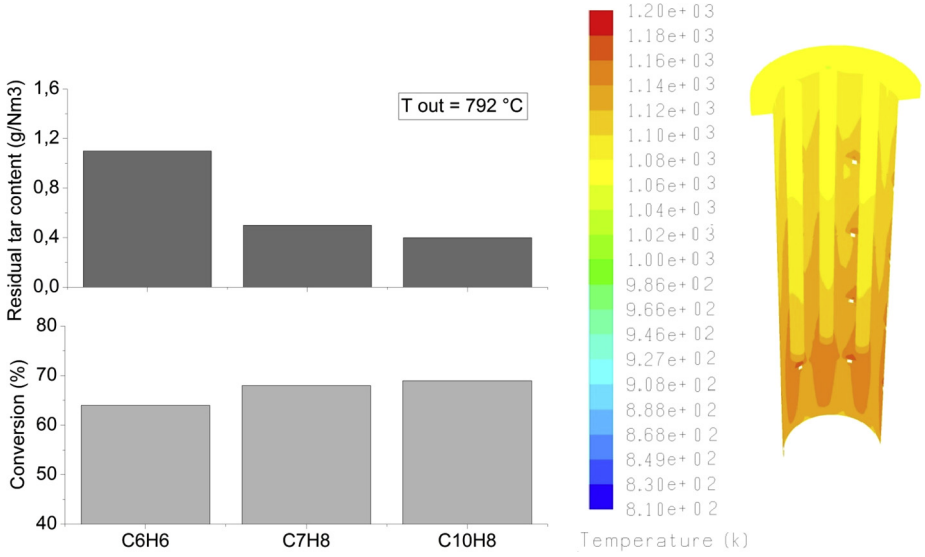

Fig. 14. a) Tar conversion (left y axis) and residual tar (right y axis) and b) Temperature profiles with Fe-olivine in the bed and O_2 injections (0.065 kg/h).

O_2 were injected in the freeboard of the reactor and it was found that a slipstream of 0.36 kg/h (corresponding to 3% of the O_2 flow sent to the combustor) is enough to obtain around 77% tar conversion, with a residual tar content of 2 g/Nm^3. Additional simulations considering a gasifier bed made of Fe-olivine (a primary catalyst with better activity for gasification, assuring a lower tar content in the input raw syngas) and with a further addition of a tiny O_2 slipstream of 0.065 kg/h (0.5% of the O_2 flow sent to the combustor), showed that tar conversion reaches about 70% and the final tar content estimated in the product gas, dry and nitrogen-free, is lower than 1 g/Nm^3 (0.9 g/Nm^3).

The role played by contact time and catalytic activity, at relatively mild temperature levels, still remains to be investigated by means of the utilization of commercial catalysts specifically addressed to conversion of heavy hydrocarbons.

Acknowledgements

The authors kindly acknowledge the financial support of Project HBF 2.0, funded by the Italian Ministry of Economic Development.

References

[1] R.A.M. Esfahani, L. Osmieri, S. Specchia, S. Yusup, A. Tavasoli, A. Zamaniyan, H2-rich syngas production through mixed residual biomass and HDPE waste via integrated catalytic gasification and tar cracking plus bio-char upgrading, Chem. Eng. J. 308 (2017) 578–587, https://doi.org/10.1016/j.cej.2016.09.049.

[2] T.A. Milne, R.J. Evans, N. Abatzaglou, Biomass Gasifier "'Tars'": Their Nature, Formation, and Conversion, (1998). doi:10.2172/3726.

[3] P. Basu, Biomass gasification, pyrolysis and torrefaction, Pract. Des. Theory (2013), https://doi.org/10.1016/C2011-0-07564-6.

[4] P.V. Aravind, W. De Jong, Evaluation of high temperature gas cleaning options for biomass gasification product gas for Solid Oxide Fuel Cells, Prog. Energy Combust. Sci. 38 (2012) 737–764, https://doi.org/10.1016/j.pecs.2012.03.006.

[5] F. Di Gregorio, F. Parrillo, E. Salzano, F. Cammarota, U. Arena, Removal of naphthalene by activated carbons from hot gas, Chem. Eng. J. 291 (2016) 244–253, https://doi.org/10.1016/j.cej.2016.01.081.

[6] Gasification apparatus and method for generating syngas from gasifiable feedstock material, 2008.

[7] A. Di Carlo, D. Borello, E. Bocci, Process simulation of a hybrid SOFC/mGT and enriched air/steam fluidized bed gasifier power plant, Int. J Hydrogen Energy (2013).

[8] A. Di Carlo, E. Bocci, A. Dell'Era, Comparison by the use of numerical simulation of a MCFC-IR and a MCFC-ER when used with syngas obtained by atmospheric pressure biomass gasification, Int. J. Hydrogen Energy (2011).

[9] N.S. Shamsul, S.K. Kamarudin, N.A. Rahman, N.T. Kofli, An overview on the

production of bio-methanol as potential renewable energy, Renew. Sustain. Energy Rev. 33 (2014) 578–588, https://doi.org/10.1016/j.rser.2014.02.024.
[10] A. Molino, G. Braccio, Synthetic natural gas SNG production from biomass gasification – Thermodynamics and processing aspects, Fuel 139 (2015) 425–429, https://doi.org/10.1016/j.fuel.2014.09.005.
[11] V.S. Sikarwar, M. Zhao, P.S. Fennell, N. Shah, E.J. Anthony, Progress in biofuel production from gasification, Prog. Energy Combust. Sci. 61 (2017) 189–248, https://doi.org/10.1016/j.pecs.2017.04.001.
[12] A. Di Carlo, P.U. Foscolo, Hot syngas filtration in the freeboard of a fluidized bed gasifier: development of a CFD model, Powder Technol. 222 (2012) 117–130, https://doi.org/10.1016/j.powtec.2012.02.019.
[13] S. Rapagnà, K. Gallucci, P.U. Foscolo, Olivine, dolomite and ceramic filters in one vessel to produce clean gas from biomass, Waste Manage. (2017), https://doi.org/10.1016/j.wasman.2017.07.038.
[14] A. D'Orazio, S. Rapagnà, P.U. Foscolo, K. Gallucci, M. Nacken, S. Heidenreich, A. Di Carlo, A. Dell'Era, Gas conditioning in H2 rich syngas production by biomass steam gasification: experimental comparison between three innovative ceramic filter candles, Int. J. Hydrogen Energy 40 (2015) 7282–7290, https://doi.org/10.1016/j.ijhydene.2015.03.169.
[15] S. Rapagnà, K. Gallucci, M. Di Marcello, M. Matt, M. Nacken, S. Heidenreich, P.U. Foscolo, Gas cleaning, gas conditioning and tar abatement by means of a catalytic filter candle in a biomass fluidized-bed gasifier, Bioresour. Technol. 101 (2010) 7123–7130.
[16] S. Rapagnà, K. Gallucci, M. Di Marcello, P.U. Foscolo, M. Nacken, S. Heidenreich, M. Matt, First Al2O3 based catalytic filter candles operating in the fluidized bed gasifier freeboard, Fuel 97 (2012) 718–724, https://doi.org/10.1016/j.fuel.2012.02.043.
[17] S. Rapagna, K. Gallucci, M. Di Marcello, P.U. Foscolo, M. Nacken, S. Heidenreich, In Situ Catalytic Ceramic Candle Filtration for Tar Reforming and Particulate Abatement in a Fluidized-Bed Biomass Gasifier, (2009) 3804–3809.
[18] E. Savuto, A. Di Carlo, E. Bocci, A. D'Orazio, M. Villarini, M. Carlini, P.U. Foscolo, Development of a CFD model for the simulation of tar and methane steam reforming through a ceramic catalytic filter, Int. J. Hydrogen Energy 40 (2015), https://doi.org/10.1016/j.ijhydene.2015.04.044.
[19] F. García-Labiano, P. Gayán, L.F. de Diego, A. Abad, T. Mendiara, J. Adánez, M. Nacken, S. Heidenreich, Tar abatement in a fixed bed catalytic filter candle during biomass gasification in a dual fluidized bed, Appl. Catal. B Environ. 188 (2016) 198–206, https://doi.org/10.1016/j.apcatb.2016.02.005.
[20] Pall Corporation, Pall Gas Solid Separation Systems: Advanced Metal and Ceramic Filter Systems for Critical Gas Solid Separation Processes, 2009, http://www.pall.com/pdf/GSS.pdf.
[21] Johnson Matthey, Delivering world class Hydrogen plant performance, 2014. http://www.jmprotech.com/images-uploaded/files/JM Hydrogen Brochure.pdf.
[22] S. Rapagnà, K. Gallucci, M. Di Marcello, M. Matt, P.U. Foscolo, M. Nacken, S. Heidenreich, Characterisation of tar produced in the gasification of biomass with in situ catalytic reforming, Int. J. Chem. React. Eng. 8 (2010), https://doi.org/10.2202/1542-6580.2188.
[23] T.A. Milne, R.J. Evans, N. Abatzaglou, Biomass Gasifier " Tars ": Their Nature , Formation , and Conversion, 1998. doi:10.2172/3726.
[24] C. Li, K. Suzuki, Tar property, analysis, reforming mechanism and model for biomass gasification-An overview, Renew. Sustain. Energy Rev. 13 (2009) 594–604, https://doi.org/10.1016/j.rser.2008.01.009.
[25] C.M. Kinoshita, Y. Wang, J. Zhou, Tar formation under different biomass gasification conditions, J. Anal. Appl. Pyrol. 29 (1994) 169–181.
[26] W.A. Jacoby, S.C. Gebhard, R.L. Vojdani, Lifetime testing of catalysts for biosyngas conditioning-single versus dual catalysts comparison, 1995.
[27] S. Rapagnà, E. Savuto, A. Di Carlo, K. Gallucci, P.U. Foscolo, Integration of Biomass Gasification and Hot Gas Cleaning Processes, in: CISAP Conf. 2018, 2018.
[28] Wilke, R. Charles, Diffusional properties of multicomponent gases, Chem. Eng. Prog. 46 (1950) 95–104.
[29] R.B. Bird, W.E. Stewart, E.N. Lightfoot, Transport Phenomena, 2002. doi:10.1016/j.ijhydene.2006.08.05.
[30] H. Depner, A. Jess, Kinetics of nickel-catalyzed purification of tarry fuel gases from gasification and pyrolysis of solid fuels, Fuel 78 (1999) 1369–1377, https://doi.org/10.1016/S0016-2361(99)00067-8.
[31] D. Swierczynski, C. Courson, A. Kiennemann, Study of steam reforming of toluene used as model compound of tar produced by biomass gasification, Chem. Eng. Process. Process Intensif. 47 (2008) 508–513, https://doi.org/10.1016/j.cep.2007.01.012.
[32] T. Numaguchi, K. Kikuchi, Intrinsic kinetics and design simulation in a complex reaction network; steam-methane reforming, Chem. Eng. Sci. 43 (1988) 2295–2301, https://doi.org/10.1016/0009-2509(88)87118-5.
[33] C.R.H. de Smet, M.H.J.M. de Croon, R.J. Berger, G.B. Marin, J.C. Schouten, Design of adiabatic fixed-bed reactors for the partial oxidation of methane to synthesis gas. Application to production of methanol and hydrogen-for-fuel-cells, Chem. Eng. Sci. 56 (2001) 4849–4861, https://doi.org/10.1016/S0009-2509(01)00130-0.
[34] K. Hou, R. Hughes, The kinetics of methane steam reforming over a Ni/α-Al2O catalyst, Chem. Eng. J. 82 (2001) 311–328, https://doi.org/10.1016/S1385-8947(00)00367-3.
[35] Unifrax, Materassini Insulfrax ® LT, (n.d.) 1–2.
[36] H.C. Hottel, W.H. McAdams, Heat Transmission, McGraw-Hill, New York, 1954.
[37] B.F. Magnussen, B.H. Hjertager, On mathematical modeling of turbulent combustion with special emphasis on soot formation and combustion, Symp. Combust. (1976).
[38] F.L. Dryer, C.K. Westbrook, Simplified reaction mechanisms for the oxidation of hydrocarbon fuels in flames, Combust. Sci. Technol. 27 (1981) 31–43, https://doi.org/10.1080/00102208108946970.
[39] N.M. Marinov, C.K. Westbrook, W.J. Pitz, Detailed and global chemical kinetics model for hydrogen, Transp. Phenom. Combust (1996) 118–129.
[40] L. Wang, Z. Liu, S. Chen, C. Zheng, Comparison of different global combustion mechanisms under hot and diluted oxidation conditions, Combust. Sci. Technol. 184 (2012) 259–276, https://doi.org/10.1080/00102202.2011.635612.
[41] M. da, G. Carvalho, T. Farias, P. Fontes, Predicting radiative heat transfer in absorbing, emitting, and scattering media using the discrete transfer method, HTD, Am. Soc. Mech. Eng. (1991).
[42] M. Ilbas, The effect of thermal radiation and radiation models on hydrogen-hydrocarbon combustion modelling, Int. J. Hydrogen Energy (2005), https://doi.org/10.1016/j.ijhydene.2004.10.009.
[43] H. Hofbauer, E. Fercher, T. Fleck, R. Rauch, G. Veronik, Two years experience with the FICFB-gasification process, 10th Eur. Conf. Technol. Exhib. Wurzbg. (1998) 3–6.
[44] S.J. Yoon, Y.C. Choi, J.G. Lee, Hydrogen production from biomass tar by catalytic steam reforming, Energy Convers. Manage. 51 (2010) 42–47, https://doi.org/10.1016/j.enconman.2009.08.017.
[45] J. Ashok, S. Kawi, Steam reforming of toluene as a biomass tar model compound over CeO 2 promoted Ni/CaOeAl2O3 catalytic systems, Int. J. Hydrogen Energy 38 (2013) 13938–13949, https://doi.org/10.1016/j.ijhydene.2013.08.029.
[46] F. Miccio, B. Piriou, G. Ruoppolo, R. Chirone, Biomass gasification in a catalytic fluidized reactor with beds of different materials, Chem. Eng. J. 154 (2009) 369–374, https://doi.org/10.1016/j.cej.2009.04.002.
[47] S. Rapagnà, M. Virginie, K. Gallucci, C. Courson, M. Di Marcello, A. Kiennemann, P.U. Foscolo, Fe/olivine catalyst for biomass steam gasification: preparation, characterization and testing at real process conditions, Catal. Today 176 (2011) 163–168, https://doi.org/10.1016/j.cattod.2010.11.098.
[48] M. Virginie, C. Courson, D. Niznansky, N. Chaoui, A. Kiennemann, Characterization and reactivity in toluene reforming of a Fe/olivine catalyst designed for gas cleanup in biomass gasification, Appl. Catal. B Environ. 101 (2010) 90–100, https://doi.org/10.1016/j.apcatb.2010.09.011.